Title

LiDAR-derived snowpack data sets from mixed conifer forests across the Western United States

Journal

Water Resources Research, 50(3)

ISSN

0043-1397

Authors

Harpold, AA

Guo, Q

Molotch, N

et al.

Publication Date

2014-03-01

DOI

10.1002/2013wr013935

Peer reviewed

AGU PUBLICATIONS

Water Resources Research

DATA AND ANALYSIS NOTE

10.1002/2013WR013935

Key Points:
- LiDAR-derived snow depth from Western United States sites are publicly available
- Research catchments had variable forest properties and snow depths among sites
- LiDAR-derived snow depths were comparable to in situ measurements

Supporting Information:
- Readme
- Figures S1 and S2

Correspondence to:
A. A. Harpold,
adrian.harpold@gmail.com

Citation:
Harpold, A. A., et al. (2014), LiDAR-derived snowpack data sets from mixed conifer forests across the Western United States, *Water Resour. Res.*, *50*, 2749–2755, doi:10.1002/2013WR013935.

Received 11 APR 2013
Accepted 27 FEB 2014
Accepted article online 3 MAR 2014
Published online 14 MAR 2014

LiDAR-derived snowpack data sets from mixed conifer forests across the Western United States

A. A. Harpold[1], Q. Guo[2], N. Molotch[1,3], P. D. Brooks[4], R. Bales[2], J. C. Fernandez-Diaz[5], K. N. Musselman[6,7], T. L. Swetnam[8], P. Kirchner[2,9], M. W. Meadows[2], J. Flanagan[2], and R. Lucas[2]

[1]Institute for Arctic and Alpine Research, University of Colorado, Boulder, Colorado, USA, [2]Sierra Nevada Research Institute, University of California Merced, Merced, California, USA, [3]Jet Propulsion Laboratory, Pasadena, California, USA, [4]Hydrology and Water Resources, University of Arizona, Tucson, Arizona, USA, [5]National Center for Airborne Laser Mapping, Houston, Texas, USA, [6]Civil and Environmental Engineering, University of California, Los Angeles, California, USA, [7]Now at Centre for Hydrology, University of Saskatchewan, Saskatoon, Saskatchewan, Canada, [8]School of Natural Resources and the Environment, University of Arizona, Tucson, Arizona, USA, [9]Now at Joint Institute for Regional Earth System Science and Engineering, University of California, Los Angeles, California, USA

Abstract Airborne-based Light Detection and Ranging (LiDAR) offers the potential to measure snow depth and vegetation structure at high spatial resolution over large extents and thereby increase our ability to quantify snow water resources. Here we present airborne LiDAR data products at four Critical Zone Observatories (CZO) in the Western United States: Jemez River Basin, NM, Boulder Creek Watershed, CO, Kings River Experimental Watershed, CA, and Wolverton Basin, CA. We make publicly available snow depth data products (1 m^2 resolution) derived from LiDAR with an estimated accuracy of $<$30 cm compared to limited in situ snow depth observations.

1. Introduction

Seasonal mountain snowpacks are the major source of water for human and natural systems in the semiarid Western United States [*Bales et al.*, 2006]. The interactions between vegetation, topography, and climate play a central role in the accumulation, ablation, and partitioning of snowpacks to the atmosphere versus infiltration and runoff. Local canopy structure (i.e., canopy density, height, etc.) at the tree and stand scale strongly controls snowpack accumulation and ablation [*Golding and Swanson*, 1986*; Molotch et al.*, 2009; *Varhola et al.*, 2010; *Varhola and Coops*, 2013]. Light Detection and Ranging (LiDAR) data sets from airborne platforms are increasingly used to estimate snow depth at high resolution ($<$1 m^2) over landscape scales ($>$100 km^2) by differencing "snow-covered" and "snow-free" elevation products [*Hopkinson et al.*, 2004*; Deems et al.*, 2006*; Trujillo et al.*, 2007*; DeBeer and Pomeroy*, 2010*; Grünewald et al.*, 2013*; Varhola and Coops*, 2013].

The goal of this paper is to present high quality, publicly available LiDAR-derived snow depth data products from four U.S. National Science Foundation Critical Zone Observatory (CZO) sites that cover a gradient of hydroclimate and snow processes in the Western United States. The CZO sites include forested research catchments where intensive ecological and hydrological measurements are currently being made.

2. Site Description

We describe LiDAR data products from four CZO sites: Jemez River Basin (JRB), Boulder Creek Watershed (BCW), Kings River Experimental Watershed (KREW), and Wolverton Basin (WLVB). The four LiDAR extents vary in size and land cover (Figure 1), but are generally topographically complex with steep drainages containing mixed conifer forests and alpine areas with seasonal snowpacks. A total of seven catchments were investigated across the four CZO sites; two each in BCW, JRB, KREW, and one from WLVB (Table 1). Detailed information and photographs of the sites are available on the CZO website (http://www.criticalzone.org, accessed 1 October 2013). The BCW site had the largest snow-covered LiDAR extent ($>$400 km^2) with forests comprised of ponderosa pine (*Pinus ponderosa*), subalpine fir (*Abies lasiocarpa*), Engelman spruce (*Picea engelmannii*), and lodgepole pine (*Pinus contorta*) at elevations $<$3000 m and rock and glacier at higher

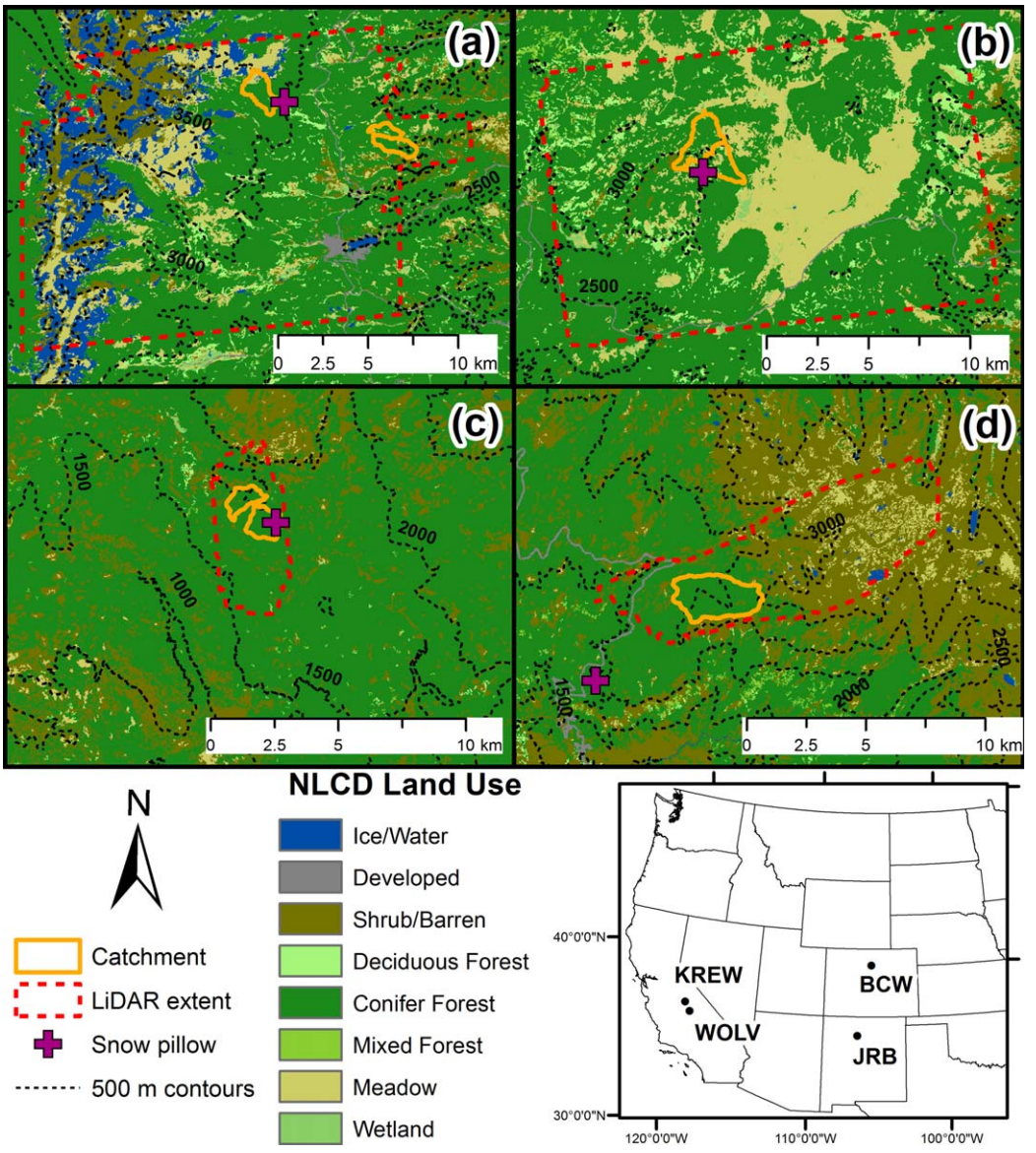

Figure 1. Overview of the snow-covered LiDAR extents for the four study sites showing the research catchments: (a) Boulder Creek Watershed, (b) Jemez River Basin, (c) Kings River Experimental Watershed, and (d) Wolverton Basin. The 2001 National Land Cover Database (NLCD) land use classifications are shown. The snow pillow locations are also shown.

elevations (Figure 1). The JRB site had a LiDAR extent of 294 km^2, with grasslands at lower elevations, transitioning to higher elevation mixed conifer forests of Douglas-fir (*Pseudotsuga menziesii*), white fir (*Abies concolor*), blue spruce (*Picea pungens*), southwestern white pine (*Pinus strobiformis*), limber pine (*Pinus flexilis*), ponderosa pine, and aspen (*Populus tremuloides*; Figure 1). The KREW LiDAR extent was 18 km^2 consisting of rock outcrops and Sierra Nevada mixed conifer forests of white fir, Jeffrey pine (*Pinus jeffreyi*), ponderosa pine, sugar pine (*Pinus lambertiana*), incense-cedar (*Calocedrus decurrens*), California black oak (*Quercus kelloggii*), and a minor component of lodgepole pine (Figure 1). The WLVB site had a snow-covered extent of 59 km^2, with red fir forest at lower elevations, transitioning to California mixed subalpine and alpine at higher elevations (Figure 1). Red fir forests species consist of red fir (*Abies magnifica*), lodgepole pine, western white pine (*Pinus monticola*), and incense-cedar. California mixed subalpine consists of large rock outcrops and scattered Jeffery pine, red fir, western white pine, and lodgepole pine. Differences in winter climates were typified by the differences in maximum snow water equivalent (SWE) in 2010 and "winter" (October through April) precipitation (P) and temperature (T) over 5 years (Table 1). The climate

Table 1. Properties Derived From the Snow-Free and Snow-Covered LiDAR Flights at the Four CZO Sites: Jemez River Basin (JRB), Boulder Creek Watershed (BCW), Kings River Experimental Watershed (KREW), and Wolverton (WLVB) and Their Corresponding Research Catchments

Site	BCW, CO	JRB, NM	KREW, CA	WLVB, CA
Snow-covered area (km^2)	261[1], 280[2]	294	18	59
Forest cover fraction (%)	35.0	47.8	57.1	25.0
Forest height (m)	7	11	14	15
Average Winter P (cm)	45.2[a], 27.5[b]	37.1[c]	126.8[e]	84.0[f]
Average winter T (cm)	−2.7[a]	−2.2[c]	4.2[e]	4.8[f]
Snow-free flight date	8/21-8/26/2010	6/29-7/8/2010	8/5-8/15/2010	8/5-8/15/2010
Snow-covered flight date	5/5[1], 5/20/2010[4/1/2010]	4/1/2010	3/20/2010	3/21-3/22/2010
Max SWE date	4/8/2010[a]	3/29/2010[d]	4/22/2010[e]	3/15[f], 4/14/10[g]
2010 max SWE (cm)	31.8[a]	30.4[d]	86.4[e]	59.4[f], 121.8[g]

Catchment	Como[2]	Gordon[1]	History	Jaramillo	P301	P304	Wolverton
Area (km^2)	2.42	2.62	2.42	3.05	0.99	1.32	5.40
Elevation (m)	3221	2617	2947	2925	1974	1898	2525
Slope (°)	12.8	15.4	7.6	8.4	13.8	15.2	21.1
Aspect (degree CW from N)	152	153	125	202	196	230	214
Forest cover fraction (%)	46.9	52.7	49.5	43.7	69.3	60.2	53.1
Forest height (m)	6.4	3.5	10.4	8.9	16.0	14.5	17.1
Canopy point density (%)	55	54	66	66	75	75	71

Average Winter T and P refer to the period of 1 October to 1 May for water years 2006–2010. [1] refers to 5 May 2010 in Gordon Gulch and [2] to 20 May 2010 in Como. Date and amount of maximum SWE was estimated at a nearby snow pillow at each site (Figure 1):
[a]refers to the Niwot SNOTEL,
[b]to Sugarloaf NADP site,
[c]to VCNP Redondo station,
[d]to VCNP COSMOS station,
[e]to Upper Providence station, and
[f]Giant Forest station.
[g]Farewell Gap station.

observations suggest wetter ($P > 80$ cm) and warmer ($T > 4°C$) winters at the Sierra Nevada sites (KREW and WLVB) compared to colder ($T < -2°C$), drier ($P < 45$ cm) Rocky Mountain sites (BCW and JRB).

3. Data Description

3.1. LiDAR and Field Data Collection

The National Center for Airborne Laser Mapping (NCALM) employed an Optech Airborne Laser Terrain Mapper sensor (Gemini S/N 06SEN195) mounted to a twin-engine Piper PA-31 Chieftain (N931SA or N31PR) for the snow-covered flights. The system was configured with pulse repetition frequency of 100 kHz, a scanning frequency of 60 Hz, scan angle of ±14°, scan overlap of 50%, and a beam divergence of 0.25 mrad which yielded a laser footprint diameter of 15–20 cm. NCALM has typical nominal elevation accuracy of 5–10 cm with a horizontal uncertainty of 20–40 cm over flat open surfaces. The total return density for the snow-covered flights varied from 7.8 returns/m^2 at BCW on 5 May 2010, 9.1 returns/m^2 at JRB and BCW on 20 May 2010, 9.5 returns/m^2 at WLVB, and 10.3 returns/m^2 at KREW. The objective of the LiDAR flights was to measure near-peak snow accumulation for water balance estimates at each site; however, due to the elevation ranges and logistical consideration, all flights occurred after melt had begun at some locations within each extent. The timing of maximum SWE at nearby snow pillows indicates when snowmelt began relative to flight timing (Table 1). Snow-covered flights were made over 1–2 consecutive days, with the exception of BCW. Two flights were completed on 5 and 20 May 2010 and combine to cover the full BCW extent. The extent of the snow-free LiDAR data sets exceeded the snow-covered extent in all cases.

In situ snow depth measurements from ultrasonic snow depth sensors installed perpendicular to the snow surface and configured in open and under-canopy positions were used as a verification data set (see *Molotch et al.* [2009] for configuration). The average snow depth from 12:00 to 13:00 on the day of each LiDAR flight was used. Observations from continuous snow depth sensors were within 10 cm of manual measurements at peak snow depth in BCW-Como, but accuracy can vary based on sensor height and snow surface topography. The slope and aspect of sensor locations varied within and between sites, with flatter sites at BCW-Como, JRB-History, and KREW-P303, and steeper slopes sampled at BCW-Gordon, KREW-P301,

Table 2. Properties of the In Situ Sensor Snow Depths and LiDAR-Derived Snow Depths at Seven Research Catchments[a]

Site	BCW, CO		JRB, NM		KREW, CA		WLVB, CA
Catchment	Como[2]	Gordon[1]	History	Jaramillo	P301	P303	Wolverton
Snow depth (cm)	59 ± 41	7 ± 8	63 ± 26	84 ± 30	124 ± 52	97 ± 43	222 ± 50
Mask area (% of total area)	15.7	11.4	11.2	10.5	24.3	26.7	23.0
Snow depth sensors							
Measured snow depth (cm)	77 ± 23	0 ± 0	83 ± 19	N/A	172 ± 58	135 ± 61	274 ± 13
Number of sensors	16	5	9	N/A	13	5	12
Slope (°)	1–11	16–27	0–7	N/A	3–22	3–9	5–26
Canopy point density	36	38	21	N/A	48	20	34
LiDAR snow depth (cm)	62 ± 22	6 ± 4	71 ± 14	N/A	166 ± 59	125 ± 53	276 ± 27
Overall RMSE (cm)	27	7	22	N/A	18	31	23

[a]Numbers following the ± symbol refer to one standard deviation. Properties of snow depth, slope, and canopy point density were derived from the 1 m grid cell corresponding to each snow depth sensor. [1] refers to 5 May 2010 in Gordon Gulch and [2] to 20 May 2010 in Como.

and WLVB-Wolverton (Table 2). Snow water equivalent (SWE) measurements were obtained from local snow pillows (Figure 1 and Table 1).

3.2. LiDAR Data Processing

The initial LiDAR processing steps involved developing a smoothed best-estimate trajectory (SBET) and geolocation information for each return using trajectories calculated with a differential 3-D global navigation system (GNSS). Each point was classified as ground or nonground (vegetation, building, etc.) using

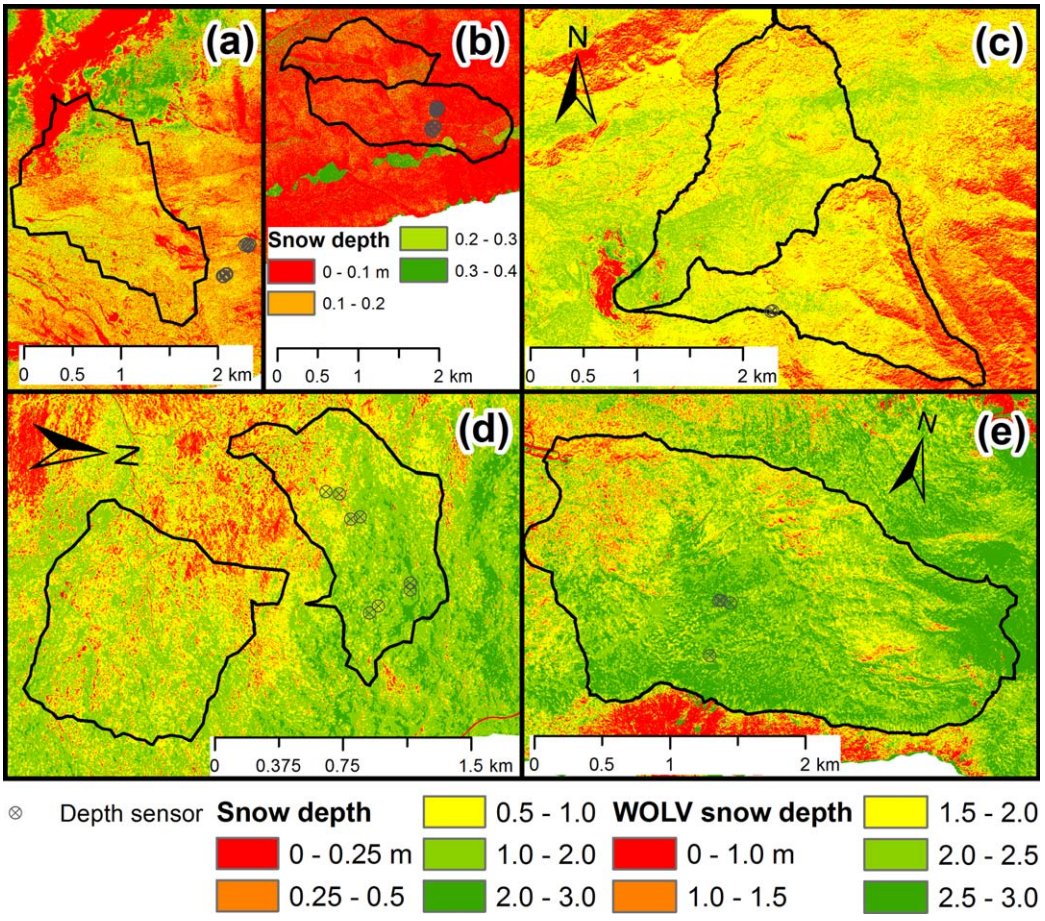

Figure 2. Snow depth at 1 m resolution for the study catchments: (a) BCW-Como, (b) BCW-Gordon, (c) JRB-Jaramillo and JRB-History, (d) KREW-P301 and KREW-P303, and (e) WLVB-Wolverton. The locations of the in situ snow depth sensors are also shown. Note that the figures have been rotated for ease of display.

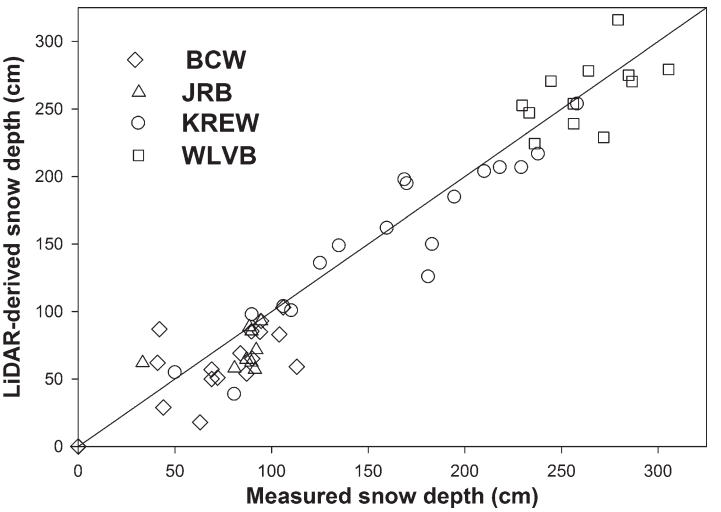

Figure 3. Comparison between LiDAR-derived snow depths versus in situ sensor values at the four study sites (symbols). All 60 sensors had a RMSE of 23 cm and r^2 of 0.97 ($p < 0.00001$).

Terrasolid's TerraScan™. The ASPRS LAS standard format version 1.2) tiles for snow-covered and snow-free flights are available via OpenTopography (http://www.opentopography.org, accessed 22 March 2013) using the DOI numbers cited (BCW (snow free): 10.5069/G93R0QR0, JRB (snow free): 10.5069/G9RB72JV, JRB (snow covered): 10.5069/G9W37T86, KREW and WOLV (snow free): 10.5069/G9BP00QB, KREW and WOLV (snow covered): 10.5069/G9BP00QB).

A simpler data product was derived from the LAS point cloud by binning the full 3-D data into regularly spaced 2.5-D grids (x, y, and elevation). The first classification used TerraScan's isolated return routine (*TerraScan User's Guide*, 2012, https://www.terrasolid.com/download/tscan.pdf) to define outliers 2 m below the ground surface by specifying a 3-D search radius and a minimum number of neighbors. The classification was completed by running TerraScan's classify ground routine, which is an iterative algorithm similar to *Axelsson* [2000] that starts with the lowest elevation return within each grid cell. The grid spacing is defined so that the return with the minimum elevation is likely to be a ground return within an area that varied between 60 and 120 m in forested terrain. Next, a triangulated faceted surface was built using the lowest returns (assumed ground) as vertices. Then the vertical distance and angle from the facet was computed and compared against user-defined filter thresholds to determine if the point can be classified as a ground or nonground return. The threshold values depend on the local terrain and are manually tuned by the NCALM data processor as filter parameters for each project area.

NCALM utilized ordinary Kriging interpolation [*Kraus and Pfeifer*, 1998] to produce two standard 1 m gridded deliverables from the point cloud data: a bare-earth digital terrain model (DTM) and a first return (top of canopy) digital surface model (DSM). Differencing the snow-free DSM by the snow-free DTM produced the canopy height model (CHM) that was used to compare vegetation between sites. The snow depth data set was the difference between the snow-covered and snow-free DTMs. The result from this differencing procedure was filtered to replace any negative snow depths with zero and remove outliers greater than 10 m. Verification of zero snow depths would benefit from simultaneous high-resolution aerial imagery, which was unavailable for this data set. The maximum snow depth of 10 m was chosen based on over a decade of snow surveys in the alpine areas of BCW and WLVB [*Jepsen et al.*, 2012]. A 1 m grid cell was determined to be forest covered if the CHM was >2 m. Canopy point density was estimated from the snow-free LiDAR point cloud as the fraction of the total returns that were >2 m higher than the snow-free DTM in each 1 m grid cell. A mask layer was developed using the snow-covered LiDAR point cloud for 1 m grid cells that did not contain returns classified as ground (e.g., snow surface). Grid cells in the mask had no direct snow surface elevation information and were thus interpolated from nearby locations.

3.3. Catchment-Scale Vegetation and Snow Depth Data Sets

The seven research catchments range from 1.0 to 5.4 km^2 and were more comparable in terms of topography and vegetation than the full snow-covered LiDAR extent (Figures 1 and 2 and Table 1). Tree height and species varied between catchments, while forest cover fraction ranged from 44% to 69% (Table 1). Both forest cover fraction and forest canopy point density were greatest at KREW-P301 and KREW-P303 while the forest canopy was tallest at WLVB-Wolverton. The forest cover fraction values were similar between the BCW and JRB catchments (Table 1), with slightly higher canopy point density values at JRB

than BCW. Average forest height was much shorter in BCW catchments versus the KREW and WLVB catchments. It should be noted that forest canopy height reported in Table 1 is not equivalent to tree height and is dependent on the surrounding forest cover fraction and canopy point density. The percentage of masked area (e.g., no snow surface returns) varied considerably based on forest canopy structure. Not surprisingly the largest masked areas >23% were in KREW-P301 and KREW-P303 where forest cover fraction and canopy point density were greatest (Table 2). Conversely, the masked areas were <16% in JRB-History, JRB-Jaramillo, and BCW-Gordon (Table 2).

Mean LiDAR-derived catchment-scale snow depths varied from 7 to 222 cm (Table 2) and mean snow depths from in situ sensors varied from 0 to 274 cm, with in situ snow depths 19%–28% greater than catchment averages (Figure 2 and Table 2), excluding BCW-Gordon that lacked snow. Catchment-scale snow depth variability was greater than in situ snow depth variability except in KREW-P301 and KREW-P303 (Table 2). The in situ sensors failed to capture the LiDAR-derived mean catchment-scale snow depth despite the installation in variable canopy positions.

3.4. Verification of LiDAR-Derived Snow Depth

LiDAR-derived snow depth error was estimated by comparing each in situ sensor measurement to its corresponding 1 m grid cell snow depth. The Root Mean Square Error (RMSE) of the LiDAR-derived snow depths was 23 cm and the r^2 was 0.97 ($p < 0.0001$) compared to measurements from 60 snow depth sensors (Figure 3). The RMSE varied from 7 to 31 cm among the catchments, which had between 5 and 16 snow sensors each (Table 2 and Figure 3). The RMSE was 31 cm at KREW-P303 and only 18 cm at the adjacent, and topographically similar, KREW-P301 catchment (Table 2). Error estimated from these point-to-point snow depth comparisons was not biased by topographic slope; however, uncertainty in elevation would be expected to increase on steeper slopes [*Deems et al*., 2013]. Snow depth RMSE values <10 cm were within the in situ sensor measurement error making verification difficult at shallower depths. Vertical errors below 30 cm are consistent with previous verification efforts in alpine areas [*Geist and Stotter*, 2008*; Moreno-Banos et al*., 2009*; DeBeer and Pomeroy*, 2010*; Joerg et al*., 2012] and similar to verification across smaller forested extents [*Reutebuch et al*., 2003*; Hopkinson et al*., 2004*; Hopkinson et al*., 2010].

4. Summary and Conclusion

The LiDAR-derived snow depth and vegetation gridded data products from the four Western United States CZO sites are publicly available (ftp://snowserver.colorado.edu/pub/WesternCZO_LiDAR_data), as well as the raw LiDAR point cloud (http://www.opentopography.org via individual DOI cited). To improve the usability of the data sets, we briefly described the site characteristics, forest type and structure, snow depth mean and variance at the catchment scale, and verified LiDAR snow depths against in situ sensor measurements. Our verification efforts showed LiDAR-derived depths had a RMSE of 23 cm compared to data from 60 snow depth sensors, which is generally acceptable for most research and resource management applications. Investigations of snow depth error sources are needed to identify locations and conditions most appropriate for airborne LiDAR applications. For example, our results suggest that differences in forest canopy structure among catchments resulted in a twofold difference in spatially interpolated under-canopy snow depths (e.g., mask area). We suggest future LiDAR-derived snow depth verification efforts use larger field verification data sets with more precise instruments (<10 cm vertical RMSE) to determine the sources of LiDAR error, including concurrent terrestrial LiDAR scans and aerial orthophotography with multispectral bands capable of verifying snow presence and absence. Newly available full waveform LiDAR is not limited by the number of discrete returns and therefore, offers another potentially unexplored data set for verifying under-canopy snow depths.

As the economic and processing limitations of acquiring LiDAR data decrease [*Stennett*, 2004], publicly available LiDAR-derived snow depth and vegetation products will become more prevalent. Here we showed limited in situ sensor measurements do not capture the mean and variance of catchment-scale snow depth. This is an important demonstration of the utility of airborne LiDAR-derived snow data products with implications for water resources management [*Hopkinson et al*., 2012], snow cover modeling [*DeBeer and Pomeroy*, 2010], and postdisturbance hydrology [*Harpold et al*., 2014]. Better linkages between in situ

observations and LiDAR data sets, at sites like the CZOs, have the potential to improve our predictions of water and energy fluxes at the landscape scale.

Acknowledgments
This research was supported by the National Science Foundation to QG for the collection of the LiDAR data (EAR 0922307), to other coauthors in support of CZO sites (EAR 724960, 725097, 724958), and EAR 1141764 and USDA grant 2012–67003-19802. The first author was supported by an NSF EAR Postdoctoral Fellowship (EAR 1144894).

References

Axelsson, P. (2000), DEM generation from laser scanner data using adaptive tin models, *International Archives of Photogrammetry and Remote Sensing, XXXIII*, Part B3, 85–92.

Bales, R., N. P. Molotch, T. H. Painter, M. D. Dettinger, R. Rice, and J. Dozier (2006), Mountain hydrology of the western United States, *Water Resour. Res.*, *42*, W08432, doi:10.1029/2005WR004387.

DeBeer, C. M., and J. W. Pomeroy (2010), Simulation of the snowmelt runoff contributing area in a small alpine basin, *Hydrol. Earth Syst. Sci.*, *7*, 971–1003, doi:10.5194/hess-14-1205-2010.

Deems, J. S., S. R. Fassnacht, and K. J. Elder (2006), Fractal distribution of snow depth from LiDAR data, *J. Hydrometeorol.*, *7*(2), 285–297, doi:10.1175/JHM487.1.

Deems, J. S., T. H. Painter, and D. C. Finnegan (2013), Lidar measurement of snow depth: A review, *J. Glaciol.*, *59*(215), 467–479, doi:10.3189/2013JoG12J154.

Geist, T., and J. Stotter (2008), Documentation of glacier surface elevation change with multi-temporal airborne laser scanner data—Case study: Hintereisferner and Kesselwandferner, Tyrol, Austria, *Z. Gletscherkd. Glazialgeol.*, *41*, 77–106.

Golding, D. L., and R. H. Swanson (1986), Snow distribution patterns in clearings and adjacent forest, *Water Resour. Res.*, *22*(13), 1931–1940, doi:10.1029/WR022i013p01931.

Grünewald, T., J. Stötter, J. W. Pomeroy, R. Dadic, I. M. Baños, J. Marturià, and M. Lehning (2013), Statistical modelling of the snow depth distribution in open alpine terrain, *Hydrol. Earth Syst. Sci.*, *17*(8), 3005-3021, doi:10.5194/hess-17-3005-2013.

Harpold, A. A., J. Biederman, K. Condon, M. Merino, Y. Korganokar, T. Nan, L. L. Sloat, M. Ross, and P. D. Brooks (2014), Changes in winter season snowpack accumulation and ablation following the Las Conchas Forest Fire, *Ecohydrology*, doi:10.1002/eco.1363, in press.

Hopkinson, C., M. Sitar, L. Chasmer, and P. Treitz (2004), Mapping snowpack depth beneath forest canopies using airborne LiDAR, *Photogramm. Eng. Remote Sens.*, *70*(3), 323–330.

Hopkinson, C., J. Pomeroy, C. DeBeer, C. Ellis, and A. Anderson (2010), Relationships between snowpack depth and primary LiDAR point cloud derivatives in a mountainous environment, in *Proceedings of Remote Sensing and Hydrology Symposium*, vol. *352*, IAHS Publ., Jackson Hole, Wyoming.

Hopkinson, C., T. Collins, A. Anderson, J. Pomeroy, and I. Spooner (2012), Spatial snow depth assessment using LiDAR transect samples and public gis data layers in the Elbow River Watershed, Alberta, *Can. Water Resour. J.*, *37*, 69–87, doi:10.4296/cwrj3702893.

Jepsen, S. M., N. P. Molotch, M. W. Williams, K. E. Rittger, and J. O. Sickman (2012), Interannual variability of snowmelt in the Sierra Nevada and Rocky Mountains, United States: Examples from two alpine watersheds, *Water Resour. Res.*, *48*, W02529, doi:10.1029/2011WR011006.

Joerg, P. C., F. Morsdorf, and M. Zemp (2012), Uncertainty assessment of multi-temporal airborne laser scanning data: A case study on an Alpine glacier, *Remote Sens. Environ.*, *127*, 118–129, doi:10.1016/j.rse.2012.08.012.

Kraus, K., and N. Pfeifer (1998), Determination of terrain models in wooded areas with airborne laser scanner data, *ISPRS J. Photogramm. Remote Sens.*, *53*(4), 193–203, doi:10.1016/S0924-2716(98)00009-4.

Molotch, N. P., P. D. Brooks, S. P. Burns, M. Litvak, R. K. Monson, J. R. McConnell, and K. Musselman (2009), Ecohydrological controls on snowmelt partitioning in mixed-conifer sub-alpine forests, *Ecohydrology*, *2*, 129–142, doi:10.1002/eco.48.

Moreno-Banos, I., et al. (2009), Snowpack depth modelling and water availability from LIDAR measurements in eastern Pyrenees, paper presented at the International Snow Science Workshop ISSW Europe, Swiss Federal Institute for Forest, Snow and Landscape Research WSL, Davos, Switzerland.

Reutebuch, S. E., R. J. McGaughey, H. E. Andersen, and W. W. Carson (2003), Accuracy of a high-resolution lidar terrain model under a conifer forest canopy, *Can. J. Remote Sens.*, *29*(5), 527–535, doi:10.5589/m03–022.

Stennett, T. A. (2004), Lidar: Strap in tight, and prepare to go vertical, *Photogramm. Eng. Remote Sens.*, *70*(5), 545–548.

Trujillo, E., J. A. Ramírez, and K. J. Elder (2007), Topographic, meteorologic, and canopy controls on the scaling characteristics of the spatial distribution of snow depth fields, *Water Resour. Res.*, *43*, W07409, doi:10.1029/2006WR005317.

Varhola, A., and N. C. Coops (2013), Estimation of watershed-level distributed forest structure metrics relevant to hydrologic modeling using LiDAR and Landsat, *J. Hydrol.*, *487*, 70–86, doi:10.1016/j.jhydrol.2013.02.032.

Varhola, A., N. C. Coops, C. W. Bater, P. Teti, S. Boon, and M. Weiler (2010), The influence of ground- and lidar-derived forest structure metrics on snow accumulation and ablation in disturbed forests, *Can. J. For. Res.*, *40*, 812–821, doi:10.1139/X10-008.